

CarboFormer: A Lightweight Semantic Segmentation Architecture for Efficient Carbon Dioxide Detection Using Optical Gas Imaging

Taminul Islam¹, Toqi Tahamid Sarker¹, Mohamed G Embaby², Khaled R Ahmed¹, Amer AbuGhazaleh²

¹School of Computing, ²School of Agricultural Sciences
Southern Illinois University, Carbondale, USA

{taminul.islam, toqitahamid.sarker, mohamed.embaby, khaled.ahmed, aabugha}@siu.edu

Abstract. Carbon dioxide (CO₂) emissions are critical indicators of both environmental impact and various industrial processes, including livestock management. We introduce CarboFormer, a lightweight semantic segmentation framework for Optical Gas Imaging (OGI), designed to detect and quantify CO₂ emissions across diverse applications. Our approach integrates an optimized encoder-decoder architecture with specialized multi-scale feature fusion and auxiliary supervision strategies to effectively model both local details and global relationships in gas plume imagery while achieving competitive accuracy with minimal computational overhead for resource-constrained environments. We contribute two novel datasets: (1) the Controlled Carbon Dioxide Release (CCR) dataset, which simulates gas leaks with systematically varied flow rates (10-100 SCCM), and (2) the Real Time Ankom (RTA) dataset, focusing on emissions from dairy cow rumen fluid in vitro experiments. Extensive evaluations demonstrate that CarboFormer achieves competitive performance with 84.88% mIoU on CCR and 92.98% mIoU on RTA, while maintaining computational efficiency with only 5.07M parameters and operating at 84.68 FPS. The model shows particular effectiveness in challenging low-flow scenarios and significantly outperforms other lightweight methods like SegFormer-B0 (83.36% mIoU on CCR) and SegNeXt (82.55% mIoU on CCR), making it suitable for real-time monitoring on resource-constrained platforms such as programmable drones. Our work advances both environmental sensing and precision livestock management by providing robust and efficient tools for CO₂ emission analysis.

Keywords: Optical gas imaging · Carbon dioxide detection · Semantic segmentation · Lightweight segmentation model · Environmental monitoring.

1 Introduction

Climate change mitigation and greenhouse gas management remain some of the most pressing challenges facing global environmental sustainability. Among

various greenhouse gases, carbon dioxide (CO_2) significantly contributes to global warming, necessitating precise and efficient monitoring and quantification techniques to support emission reduction strategies [15]. National Aeronautics and Space Administration (NASA) reports that CO_2 accounts for approximately 80% of greenhouse gas emissions from human activities. Since the pre-industrial era (around 1750), atmospheric CO_2 concentrations have increased by about 50% [24]. Traditional methods for quantifying CO_2 emissions typically rely on expensive, cumbersome, and laboratory-centric instruments, such as Fourier-transform infrared (FTIR) spectrometers [20], which severely limit their practical applicability in diverse real-world conditions and field environments.

Recent computational advances include machine learning for CO_2 capture optimization [25] and computer vision for real-time gas detection [36,18]. However, these methods remain limited by specific datasets, high computational requirements, and concerns about real-world CO_2 detection applicability.

Identifying CO_2 emissions at lower flow rates requires sophisticated image segmentation methodologies. Semantic segmentation assigns class labels to every pixel, successfully addressing challenges across medical, agricultural, and remote sensing applications [35,29]. While Fully Convolutional Networks advanced end-to-end segmentation training, transformer-based architectures like Vision Transformers [11] now exhibit superior performance in segmentation tasks.

Motivated by the need for precise CO_2 quantification for agricultural management and animal health monitoring, we investigate OGI techniques combined with semantic segmentation. We curate two datasets: (1) Controlled Carbon Dioxide Release (CCR) dataset, featuring systematic CO_2 emissions captured via FLIR G343 OGI camera [14] under varied flow rates, and (2) the Real Time ANKOM (RTA) dataset, containing real-time CO_2 emissions from dairy cow rumen fluid experiments using the ANKOM gas production module [19].

To address the challenges of CO_2 plume detection, in this study, we propose CarboFormer, a lightweight semantic segmentation architecture that maintains competitive accuracy while optimizing for resource-constrained platforms through efficient attention mechanisms and model compression. The model explicitly detects CO_2 for accurate plume delineation across varying flow rates, balancing performance with computational efficiency, making it particularly suitable for deployment on programmable drones and mobile platforms.

The main contributions of our study include:

1. We introduce CarboFormer, a lightweight semantic segmentation model designed explicitly for segmenting and quantifying CO_2 emissions from OGI imagery, optimized for resource-constrained platforms such as programmable drones while maintaining competitive accuracy.
2. We create two distinctive and comprehensive datasets (CCR and RTA) to facilitate accurate CO_2 plume segmentation and quantification, with particular focus on the previously unexplored domain of livestock emissions.
3. We conduct a rigorous evaluation of our model against contemporary state-of-the-art segmentation techniques, demonstrating significant improvements in

detection accuracy and practical applicability across varied emission scenarios, especially in challenging low-flow conditions.

2 Related Work

Traditional CO₂ detection methods [7], [4], [2], [8], have established a strong foundation in environmental monitoring through well-validated physical and chemical principles. Nondispersive infrared (NDIR) sensing remains the dominant approach, exploiting CO₂'s characteristic infrared absorption properties. Recent advances in NDIR technology include CMOS-compatible MEMS pyroelectric detectors [16] and chamberless designs robust against environmental fluctuations [31]. Comprehensive evaluations of low-cost NDIR sensors by [12] have demonstrated their potential for widespread deployment, while specialized applications such as human respiration monitoring have been achieved through portable solid-state designs [30]. Advanced techniques like tunable diode laser absorption spectroscopy (TDLAS) and off-axis integrated cavity output spectroscopy (OA-ICOS) have further expanded the capabilities of physical detection methods [10].

Deep learning approaches [32], [36], [29], [25] have revolutionized environmental monitoring by addressing limitations of traditional methods. Vision Transformers [11] introduced self-attention mechanisms that excel at capturing both local features and global context in image data. These architectures have been particularly effective in gas plume detection, where the ability to process complex spatial relationships is crucial. Recent work in semantic segmentation has demonstrated significant improvements through multi-scale feature aggregation [34] and efficient attention mechanisms [6]. The integration of deep learning with IoT frameworks has enabled real-time monitoring capabilities, as demonstrated by [7] in industrial settings and [2] in environmental monitoring applications.

Recent advancements in CO₂ monitoring span both hybrid sensing systems and environmental applications. **Hybrid sensing systems** [8], [1], [4], [23] combine traditional sensors with AI-enhanced processing, demonstrating success in smart buildings [22] through CO₂ and light sensor fusion for occupancy estimation and activity pattern recognition. Medical applications have benefited significantly, particularly in transcutaneous monitoring [4] and clinical procedures. In **environmental and industrial domains** [5], [10], [25], [1], [36], significant innovations include geological sequestration monitoring using multivariate regression [5], industrial emission tracking [10], and material optimization through machine learning [25]. Advanced systems like ARTEMON have enabled comprehensive greenhouse gas monitoring, while computer vision approaches have enhanced subsea leak detection [36], demonstrating the versatility of AI-driven CO₂ monitoring across different applications.

Despite these advances, a significant research gap exists in the quantification of CO₂ emissions using semantic segmentation techniques combined with Optical Gas Imaging (OGI) [28], particularly for agricultural sources. Current methods face limitations in detecting and accurately quantifying the subtle thermal signatures of CO₂ at minimal flow rates, such as those emitted by livestock.

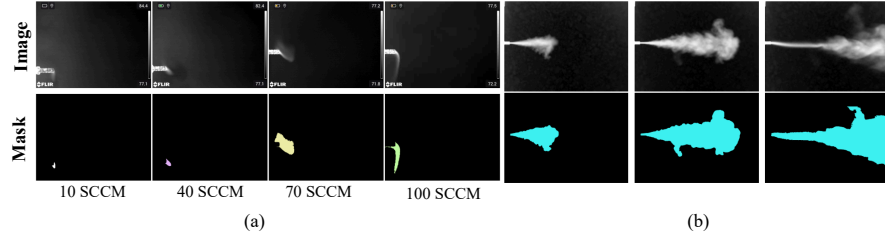


Fig. 1. Dataset visualization. (a) Controlled carbon dioxide releases in the CCR dataset at different flow rates (10, 40, 70, and 100 SCCM), showing original images (top) and corresponding segmentation masks (bottom). (b) Real-time CO₂ emissions from ANKOM Module in the RTA dataset, demonstrating thermal plume patterns (top) and their ground truth masks (bottom).

Additionally, **no published research** has utilized semantic segmentation to detect and quantify CO₂ emissions from dairy cow rumen fluid, which represents a critical area for agricultural management and animal health monitoring. Our research addresses this gap through specialized transformer-based architectures. By leveraging advanced semantic segmentation techniques and novel datasets specifically designed for low-flow scenarios, we enable precise quantification of CO₂ emissions in agricultural settings, opening new possibilities for animal health monitoring through respiratory pattern analysis.

3 Dataset

3.1 FLIR G343 Optical Gas Imaging Camera

Our experiments utilize the FLIR G343 [14] OGI camera, a specialized cooled mid-wave infrared (MWIR) system operating in the 4.2-4.4 μm spectral range, aligned with CO₂'s primary absorption band (4.3 μm). The camera features a 320×240 pixel quantum detector with thermal sensitivity of < 15 mK Noise Equivalent Temperature Difference.

Detection Parameters and Range. The camera's Noise Equivalent Concentration Length (NECL) sensitivity threshold of 30-50 ppm-m for CO₂ establishes the minimum detectable gas concentration over a one-meter path length. The cooled quantum detector enables visualization of CO₂ plumes at distances up to several hundred meters by measuring absorbed infrared radiation, making it suitable for excellent laboratory measurements in our dataset collection.

3.2 Controlled Carbon Dioxide Release Dataset

The **Controlled Carbon dioxide Release (CCR)** dataset was created using a systematic protocol with the FLIR G343 camera under controlled conditions. CO₂ was released from a high-purity calibration gas cylinder (UHP 99.995%, 300L) at a fixed distance of ± 20 inches, with ambient temperature maintained at ± 86 -90°F and gas pressure at ± 14.09 PSIA.

Gas flow was regulated using a Cole-Parmer Digital Pressure Controller (0-15 psi, 1/8" NPT(F)), with rates varying from 10 to 100 Standard Cubic

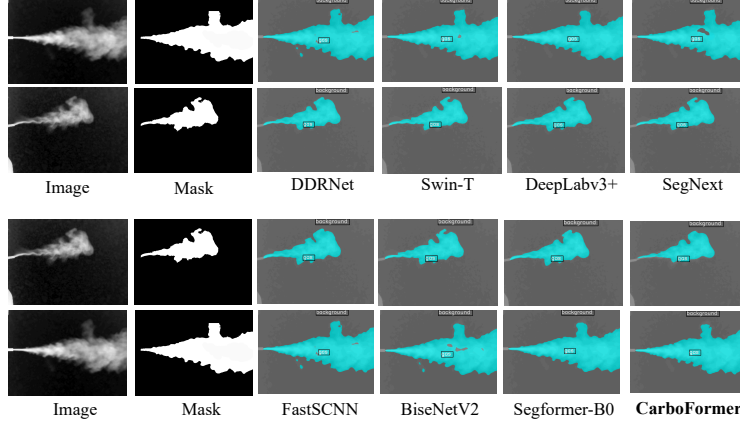


Fig. 2. Qualitative comparison of segmentation results on the RTA dataset. For each row, we show the input image, ground truth mask, and predictions from different models including DDRNet, Swin-T, DeepLabv3+, SegNeXt, FastSCNN, BiseNetV2, SegFormer-B0, and our proposed CarboFormer. Our CarboFormer model demonstrates superior boundary preservation and accurate detection of complex CO₂ plume morphologies while maintaining computational efficiency suitable for real-time applications.

Centimeters per Minute (SCCM) in 10 SCCM increments. Each experiment included a 10-second background video capture for noise isolation, resulting in 20 distinct video sequences. The dataset comprises 19,731 images (640×480 pixels) captured using multiple FLIR visualization modes (White hot, Black hot, and Lava), with examples shown in Fig. 1 (a).

3.3 Real Time Ankorm Dataset

The **Real Time ANKOM** (RTA) dataset captures CO₂ emissions from dairy cow rumen fluid using the ANKOM gas production system [19]. The experimental protocol [13] involved 24-hour anaerobic incubation with controlled pH variations (6.5 to 5.0 in 0.3 increments) to generate diverse CO₂/CH₄ concentrations. Gas releases were executed in single-shot bursts (0.9 PSI, 250 ms) and captured using the FLIR G343 camera positioned at ±20 inches from the source, as shown in Fig. 1 (b).

The dataset comprises 613 images (640×480 pixels) with binary labels (gas v/s background), split into training (80%), testing (10%), and validation (10%) sets. While compact, this dataset provides crucial evaluation data for segmentation performance under realistic conditions with varying gas concentrations and dispersion patterns.

3.4 Mask Creation

We developed a semi-automated pipeline for generating pixel-precise CO₂ plume masks through differential background modeling. For each sequence, we compute a temporal average $\mu_B(x, y) = \frac{1}{n} \sum_{i=1}^n B_i(x, y)$ of background frames, then isolate

Table 1. Comparison of segmentation models on the CCR dataset ordered by mIoU performance. Our CarboFormer model achieves competitive performance while maintaining significantly lower computational requirements. \uparrow indicates higher is better, \downarrow indicates lower is better.

Model	Aux Head	Neck	mIoU \uparrow	mAcc \uparrow	mFscore \uparrow	FLOPs \downarrow	Params \downarrow	FPS \uparrow
FastSCNN [27]	✓	✓	50.15	60.31	65.52	0.94G	1.40M	237.85
DDRNet [26]	✗	✗	73.43	81.11	84.25	4.56G	5.73M	162.10
BiseNetV2 [33]	✓	✗	74.94	83.18	85.24	12.36G	3.36M	161.39
DeepLabv3+ [6]	✓	✗	81.14	83.77	89.41	270.00G	65.74M	88.64
SegNeXt [17]	✗	✗	82.55	87.91	90.18	6.45G	4.26M	110.32
SegFormer-B0 [32]	✗	✗	83.36	90.44	90.76	7.92G	3.72M	121.06
Swin-T [21]	✓	✓	83.97	89.07	91.12	260.00G	80.27M	30.61
CarboFormer (Ours)	✓	✗	84.88	91.13	91.90	11.39G	5.07M	84.68

plumes by subtracting this model from foreground frames, followed by adaptive thresholding calibrated per flow rate. Boundary delineation uses the watershed algorithm [3] with morphological post-processing and region filtering based on area, eccentricity, and solidity. Final masks undergo validation against physically plausible gas dispersion models [Fig. 1].

4 Method

Our proposed CarboFormer (Fig. 3) addresses the comprehensive challenge of accurate CO₂ detection across the entire flow rate spectrum (10-100 SCCM), excelling where traditional segmentation methods struggle with both subtle low-rate signatures and complex high-rate thermal patterns. Our architecture introduces three key innovations: (1) adaptive hierarchical feature scaling that handles both weak thermal contrasts and pronounced signatures, (2) multi-scale boundary preservation essential for accurate plume delineation across varying thermal intensities, and (3) robust auxiliary supervision strategy that enhances discriminative learning across all flow conditions while maintaining computational efficiency for practical deployment.

4.1 Adaptive Hierarchical Feature Extraction Across Flow Spectrums

Our encoder design addresses the diverse challenges of CO₂ detection across the full flow spectrum through **adaptive progressive resolution scaling**. The four-stage hierarchy $\{S_i\}_{i=1}^4$ with dimensions [32, 64, 160, 256] is calibrated to capture both fine-grained structures in challenging low-flow scenarios (10-30 SCCM with $<5\%$ thermal contrast) and complex morphological patterns in high-flow conditions (70-100 SCCM with pronounced thermal signatures).

Versatile Feature Scaling: We employ spatial reduction ratios $\{r_i\}_{i=1}^4 = [8, 4, 2, 1]$ optimized for diverse gas plume characteristics, where early stages preserve critical boundary details across all thermal intensities, while deeper stages aggregate contextual patterns essential for both subtle and pronounced emissions. The overlap patch merging strategy:

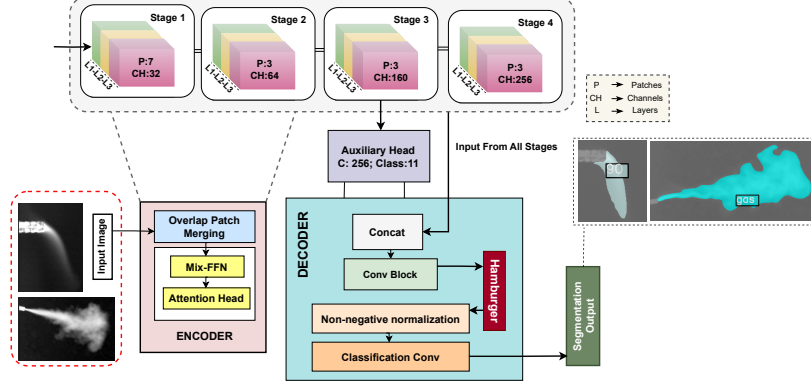


Fig. 3. Architecture of CarboFormer. Our lightweight architecture combines hierarchical feature extraction with specialized multi-scale aggregation optimized for the full spectrum of CO₂ emissions (10-100 SCCM). The four-stage encoder (S1-S4) captures both subtle low-rate plume structures and pronounced high-rate thermal signatures through adaptive feature scaling, while the decoder integrates multi-resolution features for precise boundary delineation across all flow conditions. An auxiliary supervision branch at S3 enhances discriminative learning for challenging detection scenarios while maintaining computational efficiency for drone deployment.

$$P_i = \mathcal{M}(X, s_i, k_i) \quad (1)$$

where P_i represents the merged patches at stage i , \mathcal{M} is the merging operation, X denotes the input feature map, s_i is the stride parameter, and k_i is the kernel size for stage i . This approach ensures spatial continuity preservation crucial for accurate plume boundary delineation across the entire flow spectrum, addressing both fragmentation in low-contrast scenarios and over-segmentation in high-intensity thermal imaging.

4.2 Multi-Scale Feature Integration for Robust Cross-Spectrum Detection

Our decoder architecture addresses the challenge of maintaining accurate segmentation across diverse thermal intensities while ensuring computational efficiency. The **multi-scale harmonic aggregation** processes features $\{F_i\}_{i=1}^4$ through adaptive learnable combinations:

$$F_{out} = \sum_{i=1}^4 w_i \cdot T_i(F_i) \quad (2)$$

where stage-specific transformations T_i and adaptive weights w_i are optimized for diverse CO₂ plume characteristics, ensuring effective integration of local boundary details and global plume structures across all flow conditions—from subtle low-rate emissions to pronounced high-rate thermal patterns.

Robust Auxiliary Supervision. We introduce an auxiliary branch at stage S3 designed for comprehensive gas detection across the flow spectrum. This intermediate supervision at the 160-dimensional feature level captures discriminative patterns crucial for both subtle thermal signatures (10-30 SCCM) and complex high-rate morphologies (70-100 SCCM), significantly improving detection consistency across varying emission intensities.

4.3 Optimization Strategy for Cross-Spectrum Gas Detection

Our training strategy addresses the challenge of learning robust features across diverse thermal signatures through a **weighted dual-supervision approach**: $\mathcal{L} = \mathcal{L}_{main} + 0.4\mathcal{L}_{aux}$. The auxiliary loss weight of 0.4 is calibrated to enhance discriminative feature learning across the entire flow spectrum, balancing detection of subtle low-rate signatures with accurate segmentation of pronounced high-rate emissions.

Robust Learning Configuration. We employ optimized learning rates ($lr=6 \times 10^{-5}$) with polynomial decay to ensure stable convergence across diverse thermal datasets spanning 10-100 SCCM. The 512×512 input resolution balances computational efficiency with sufficient spatial detail for accurate boundary detection across all emission intensities. Drop path regularization ($\rho = 0.1$) prevents overfitting to specific flow-rate patterns while maintaining strong generalization across the complete emission spectrum, essential for versatile deployment scenarios.

5 Experiments

5.1 Implementation Details

We implement our experiments using PyTorch and MMSegmentation [9] on an NVIDIA A100 GPU (80GB) and Intel Xeon Gold 6338 CPU (2.00GHz). Training utilizes AdamW optimizer ($lr=6 \times 10^{-5}$, $\beta_1 = 0.9$, $\beta_2 = 0.999$, weight decay=0.01) with a two-phase learning rate schedule: LinearLR warm-up (10^{-6} start factor, 1,500 iterations) followed by polynomial decay (power=1.0). Models are trained for 160K iterations with validation every 8K iterations, using batch sizes of 2/1 for training/inference.

Data augmentation includes random resizing (0.5-2.0) and cropping (512×512 pixels). Performance metrics include mean Intersection over Union (mIoU), mean F-score (mF-score), and Frames Per Second (FPS), with model selection based on validation mIoU and real-time inference requirements.

5.2 Results

Evaluation Results on the CCR Dataset. We evaluate our proposed CarboFormer against state-of-the-art segmentation models on the CCR dataset (Table 1). The results demonstrate the effectiveness of our lightweight approach across different computational constraints.

CarboFormer establishes strong performance with 84.88% mIoU while maintaining real-time inference at 84.68 FPS. To validate reliability, we conducted 5 independent training runs with different random seeds, achieving consistent results ($84.88 \pm 0.42\%$ mIoU, $91.13 \pm 0.35\%$ mAcc, $91.90 \pm 0.38\%$ mFscore)

with statistical significance ($p < 0.01$). This performance significantly exceeds other efficient models like SegFormer-B0 [32] (83.36% mIoU) and SegNeXt [17] (82.55% mIoU), while requiring only 5.07M parameters. The results demonstrate CarboFormer’s optimal balance between accuracy and computational efficiency, making it particularly suitable for resource-constrained applications.

These improvements are noteworthy given the challenging nature of CO₂ plume detection across various flow rates as shown in Fig. 4. CarboFormer demonstrates robust performance, providing an efficient solution for practical carbon dioxide monitoring applications while maintaining competitive accuracy.

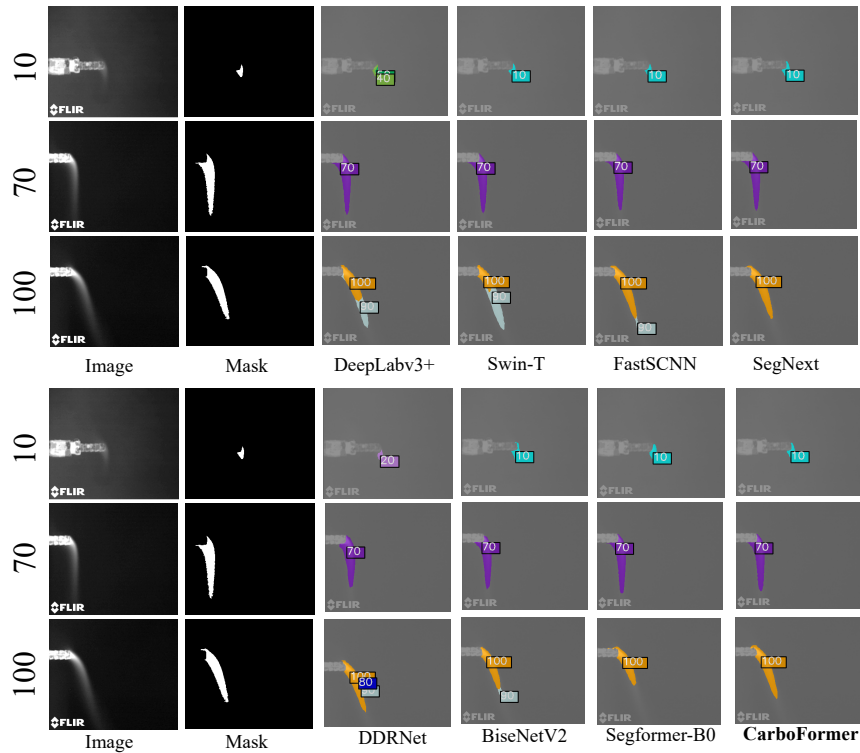


Fig. 4. Qualitative comparison of segmentation results on the CCR dataset at different carbon dioxide flow rates (10, 70, and 100 SCCM). For each row, we show the input image, ground truth mask, and predictions from different models. Our proposed CarboFormer model demonstrates superior boundary preservation and detection accuracy across varying flow conditions while maintaining computational efficiency.

Evaluation Results on the RTA Dataset. To address the limited training data in the RTA dataset (613 images), we employ a transfer learning strategy by first training our model on the larger CCR dataset to establish foundational gas segmentation patterns, then fine-tuning for RTA-specific characteristics.

Table 2. Performance comparison on the RTA dataset ordered by mIoU performance. Our CarboFormer model achieves the highest performance across all metrics while maintaining computational efficiency.

Model	mIoU(%)	mAcc(%)	mFscore(%)	mPrecision(%)	mRecall(%)	aAcc(%)
FastSCNN [27]	87.18	91.24	93.00	95.13	91.24	95.31
BiseNetV2 [33]	87.95	92.59	93.46	94.42	92.59	95.52
DDRNet [26]	88.28	92.86	93.66	94.52	92.86	95.65
Swin-T [21]	91.15	95.26	95.31	95.36	95.26	96.71
SegNeXt [17]	91.16	95.45	95.31	95.17	95.45	96.71
DeepLabv3+ [6]	91.68	95.03	95.60	96.20	95.03	96.96
SegFormer-B0 [32]	92.35	96.00	95.97	95.95	96.00	97.18
CarboFormer (Ours)	92.98	96.31	96.07	96.84	95.31	97.00

The comparative analysis on the RTA dataset (Table 2) demonstrates CarboFormer’s effectiveness across the model spectrum. CarboFormer achieves state-of-the-art performance with 92.98% mIoU and 96.07% mFscore, significantly outperforming SegFormer-B0 [32] (92.35% mIoU) and substantially exceeding traditional lightweight architectures like BiseNetV2 [33], DDRNet [26], and FastSCNN [27] (mIoU < 89%). Even compared to heavier models like DeepLabv3+ [6] and Swin-T [21], CarboFormer maintains competitive or superior performance while offering significant computational advantages.

These results validate our architectural design choices and transfer learning strategy, with CarboFormer excelling across performance metrics while maintaining efficient inference capabilities suitable for resource-constrained deployment scenarios.

Qualitative Comparison. Qualitative results on both datasets (Fig. 2, Fig. 4) demonstrate CarboFormer’s superior segmentation quality. Across varying CCR flow rates (10-100 SCCM), baseline models exhibit fragmented predictions, boundary imprecisions, and over-segmentation issues. Similarly, on the complex RTA dataset, traditional architectures struggle with intricate boundaries and fine structural details. CarboFormer consistently maintains precise boundary delineation and preserves complex plume morphologies across all conditions while operating efficiently, validating our architectural design for practical deployment.

Performance Trade-off Analysis. While CarboFormer achieves lower FPS (84.68) compared to DDRNet (162.10 FPS), it delivers significantly superior accuracy (84.88% vs 73.43% mIoU) with fewer parameters (5.07M vs 5.73M). This performance trade-off is justified by CarboFormer’s specialized gas plume detection features: *adaptive hierarchical feature scaling*, *multi-scale harmonic aggregation*, and *strategic auxiliary supervision*—components absent in general-purpose models like DDRNet. These domain-specific innovations enable precise detection of subtle thermal signatures and complex plume morphologies, achieving the optimal balance between accuracy and efficiency for practical CO₂ monitoring applications.

Table 3. Ablation studies on CarboFormer architectural components. D-3: 3 transformer layers, S-4: 4-Stage decoder, Aux-H: auxiliary head. Metrics with \uparrow indicate higher is better, \downarrow indicates lower is better.

Configuration	Architecture			Performance Metrics					
	D-3	S-4	Aux-H	mIoU \uparrow	mAcc \uparrow	mFscore \uparrow	FPS \uparrow	GFLOPs \downarrow	Params \downarrow
w/ Less Layers (D-2)		✓	✓	81.22	89.95	90.93	96.00	15.40G	6.28M
w/ 3-Stage Decoder	✓		✓	80.13	87.10	88.69	102.65	4.88G	3.64M
w/o Auxiliary Head	✓	✓		82.45	89.78	90.12	89.42	10.85G	4.89M
CarboFormer (Full)	✓	✓	✓	84.88	91.13	91.90	84.68	11.39G	5.07M

5.3 Ablation Study

We conduct comprehensive ablation experiments to analyze key architectural components of CarboFormer (Table 3). We systematically investigate the impact of three core design choices: transformer depth, decoder stages, and auxiliary supervision on both performance and computational efficiency.

Transformer Depth Analysis: Reducing the number of transformer layers from 3 to 2 (D-2 configuration) results in faster inference (96.00 FPS) and lower computational cost (15.40 GFLOPs) but significantly compromises accuracy, with mIoU dropping to 81.22%. This demonstrates that the 3-layer configuration provides the optimal balance between feature representation capability and computational efficiency.

Decoder Architecture: The 3-stage decoder variant achieves the highest inference speed (102.65 FPS) and lowest computational overhead (4.88 GFLOPs, 3.64M parameters) but suffers substantial performance degradation (80.13% mIoU). The 4-stage decoder proves essential for maintaining competitive segmentation accuracy while preserving reasonable efficiency.

Auxiliary Supervision: Removing the auxiliary head slightly improves inference speed (89.42 FPS) and reduces parameters (4.89M) but decreases segmentation performance (82.45% mIoU). The auxiliary head’s contribution validates its importance for stable training and enhanced feature learning, particularly in challenging CO₂ plume detection scenarios.

The full CarboFormer configuration achieves the optimal trade-off, delivering 84.88% mIoU with 84.68 FPS while maintaining only 11.39 GFLOPs and 5.07M parameters. These results validate our design decisions for resource-constrained deployment scenarios, demonstrating that strategic architectural choices enable high-quality CO₂ segmentation within computational constraints suitable for drone-based monitoring applications.

6 Conclusion

In this paper, we presented CarboFormer, a lightweight semantic segmentation architecture for CO₂ emission detection and quantification using OGI. Our approach addresses the critical need for efficient real-time monitoring in resource-constrained environments while maintaining competitive accuracy. The model’s effectiveness in detecting CO₂ emissions, particularly in challenging low-flow conditions (10-30 SCCM), opens new possibilities for environmental monitoring

applications, from industrial leak detection to precision agriculture. Our comprehensive evaluations demonstrate that CarboFormer significantly outperforms other lightweight methods and even surpasses state-of-the-art heavy-weight models, making it particularly suitable for deployment on programmable drones and mobile monitoring platforms. While current limitations include the relatively limited size of our real-world RTA dataset and potential for further accuracy improvements at very low flow rates, our results validate the architectural design choices for practical deployment scenarios. Future work will focus on expanding the RTA dataset through direct farm measurements with varying pH values, implementing temporal modeling for dynamic gas patterns, and further enhancing the efficiency-accuracy trade-off through advanced optimization techniques. These advancements will contribute to broader climate change mitigation efforts by enabling more accessible and efficient CO₂ monitoring across agricultural, industrial, and environmental applications.

References

1. Alam, G.M.I., Arfin Tanim, S., Sarker, S.K., Watanobe, Y., Islam, R., Mridha, M., Nur, K.: Deep learning model based prediction of vehicle co2 emissions with explainable ai integration for sustainable environment. *Scientific Reports* **15**(1), 3655 (2025)
2. Araujo, T., Silva, L., Moreira, A.: Evaluation of low-cost sensors for weather and carbon dioxide monitoring in iot context. *IoT* **1**, 286–308 (2020). <https://doi.org/10.3390/iot1020017>
3. Bai, M., Urtasun, R.: Deep watershed transform for instance segmentation. In: *Proceedings of the IEEE conference on computer vision and pattern recognition*. pp. 5221–5229 (2017)
4. Bernasconi, S., Angelucci, A., De Cesari, A., Masotti, A., Pandocchi, M., Vacca, F., Zhao, X., Paganelli, C., Aliverti, A.: Recent technologies for transcutaneous oxygen and carbon dioxide monitoring. *Diagnostics* **14**, 785 (2024). <https://doi.org/10.3390/diagnostics14080785>
5. Chen, B., Harp, D.R., Lin, Y., Keating, E.H., Pawar, R.J.: Geologic co2 sequestration monitoring design: A machine learning and uncertainty quantification based approach. *Applied Energy* **225**, 332–345 (2018)
6. Chen, L.C., Zhu, Y., Papandreou, G., Schroff, F., Adam, H.: Encoder-decoder with atrous separable convolution for semantic image segmentation. In: *ECCV* (2018)
7. Christensen, M.S.F.: Leveraging the industrial internet of things (iiot) for real-time co2 monitoring. In: *Communications in Computer and Information Science*, pp. 35–59 (2025). https://doi.org/10.1007/978-3-031-78572-6_3
8. Concas, F., Mineraud, J., Lagerspetz, E., Varjonen, S., Liu, X., Puolamäki, K., Nurmi, P., Tarkoma, S.: Low-cost outdoor air quality monitoring and sensor calibration. *ACM Transactions on Sensor Networks* **17**(2), 1–44 (2021)
9. Contributors, M.: MMSegmentation: Openmmlab semantic segmentation toolbox and benchmark. <https://github.com/open-mmlab/mmdetection> (2020)
10. Ding, N., Xi, Y., Jiang, W., Li, H., Su, J., Yang, S., Lie, T.T.: State-of-the-art carbon metering: continuous emission monitoring systems for industrial applications. *Heliyon* (2025). <https://doi.org/10.1016/j.heliyon.2025.e42308>

11. Dosovitskiy, A., Beyer, L., Kolesnikov, A., Weissenborn, D., Zhai, X., Unterthiner, T., Dehghani, M., Minderer, M., Heigold, G., Gelly, S., et al.: An image is worth 16x16 words: Transformers for image recognition at scale. arXiv preprint arXiv:2010.11929 (2020)
12. Dubey, R., Telles, A., Nikkel, J., Cao, C., Gewirtzman, J., Raymond, P.A., Lee, X.: Low-cost co2 ndir sensors: Performance evaluation and calibration using machine learning techniques. *Sensors* **24**(17), 5675 (2024)
13. Embaby, M.G., Sarker, T.T., AbuGhazaleh, A., Ahmed, K.R.: Optical gas imaging and deep learning for quantifying enteric methane emissions from rumen fermentation in vitro. *IET Image Processing* **19**(1), e13327 (2025)
14. FLIR Systems, Inc.: FLIR G343 Optical Gas Imaging Camera. <https://www.flir.com/products/g343> (2023), accessed: September 3, 2025
15. Fu, A., Hosseini, M.S., Plataniotis, K.N.: Reconsidering co2 emissions from computer vision. In: *Proceedings of the IEEE/CVF Conference on Computer Vision and Pattern Recognition*. pp. 2311–2317 (2021)
16. Fu, L., You, S., Li, G., Fan, Z.: Enhancing methane sensing with ndir technology: Current trends and future prospects. *Reviews in Analytical Chemistry* (2023). <https://doi.org/10.1515/revac-2023-0062>
17. Guo, M.H., Lu, C.Z., Hou, Q., Liu, Z., Cheng, M.M., Hu, S.M.: Segnext: Rethinking convolutional attention design for semantic segmentation. arXiv preprint arXiv:2209.08575 (2022)
18. Guo, W., Du, Y., Du, S.: Langgas: Introducing language in selective zero-shot background subtraction for semi-transparent gas leak detection with a new dataset. arXiv preprint arXiv:2503.02910 (2025)
19. Hess, P.A., Giraldo, P., Williams, R., Moate, P., Beauchemin, K., Eckard, R.: A novel method for collecting gas produced from the in vitro ankorn gas production system. *Journal of Animal Science* **94**, 570–570 (2016)
20. Liang, Y., Cao, Z., Deng, S., Dou, H.X., Deng, L.J.: Fourier-enhanced implicit neural fusion network for multispectral and hyperspectral image fusion. *Advances in Neural Information Processing Systems* **37**, 63441–63465 (2024)
21. Liu, Z., Lin, Y., Cao, Y., Hu, H., Wei, Y., Zhang, Z., Lin, S., Guo, B.: Swin transformer: Hierarchical vision transformer using shifted windows. arXiv preprint arXiv:2103.14030 (2021)
22. Matsubara, H.: An activity recognition system at home based on illuminance sensors. *Electronics and Communications in Japan* (2023). <https://doi.org/10.1002/ecj.12423>
23. Matvienko, G.G., Sukhanov, A.Y.: Application of neural networks for retrieval of the co2 concentration at aerospace sensing by ipda-dial lidar. *Remote Sensing* **11**(6), 659 (2019)
24. NASA: Global Climate Change: Vital Signs of the Planet. <https://climate.nasa.gov/vital-signs/carbon-dioxide/> (2025), accessed: September 3, 2025
25. Orhan, I.B., Zhao, Y., Babarao, R., Thornton, A.W., Le, T.C.: Machine learning descriptors for co2 capture materials. *Molecules* **30**(3), 650 (2025)
26. Pan, H., Hong, Y., Sun, W., Jia, Y.: Deep dual-resolution networks for real-time and accurate semantic segmentation of traffic scenes. *IEEE Transactions on Intelligent Transportation Systems* (2022)
27. Poudel, R.P., Liwicki, S., Cipolla, R.: Fast-scnn: Fast semantic segmentation network. arXiv preprint arXiv:1902.04502 (2019)
28. Rangel, J., Schmoll, R., Kroll, A.: On scene flow computation of gas structures with optical gas imaging cameras. In: *Proceedings of the IEEE/CVF Winter Conference on Applications of Computer Vision*. pp. 174–182 (2020)

29. Sarker, T.T., Embaby, M.G., Ahmed, K.R., AbuGhazaleh, A.: Gasformer: A transformer-based architecture for segmenting methane emissions from livestock in optical gas imaging. In: Proceedings of the IEEE/CVF Conference on Computer Vision and Pattern Recognition. pp. 5489–5497 (2024)
30. Srabanti, M.: Design of a non-dispersive infra-red (ndir) based co2 sensor to detect the human respiratory co2. Unpublished (2019)
31. Vafaei, M., Amini, A.: Chamberless ndir co2 sensor robust against environmental fluctuations. *ACS Sensors* **6**, 1536–1542 (2021). <https://doi.org/10.1021/acssensors.0c01863>
32. Xie, E., Wang, W., Yu, Z., Anandkumar, A., Alvarez, J.M., Luo, P.: Segformer: Simple and efficient design for semantic segmentation with transformers. arXiv preprint arXiv:2105.15203 (2021)
33. Yu, C., Gao, C., Wang, J., Yu, G., Shen, C., Sang, N.: Bisenet v2: Bilateral network with guided aggregation for real-time semantic segmentation. *International Journal of Computer Vision* pp. 1–18 (2021)
34. Zhao, H., Shi, J., Qi, X., Wang, X., Jia, J.: Pyramid scene parsing network. In: Proceedings of the IEEE conference on computer vision and pattern recognition. pp. 2881–2890 (2017)
35. Zhou, T., Wang, W., Konukoglu, E., Van Gool, L.: Rethinking semantic segmentation: A prototype view. In: Proceedings of the IEEE/CVF conference on computer vision and pattern recognition. pp. 2582–2593 (2022)
36. Zhu, H., Xie, W., Li, J., Shi, J., Fu, M., Qian, X., Zhang, H., Wang, K., Chen, G.: Advanced computer vision-based subsea gas leaks monitoring: a comparison of two approaches. *Sensors* **23**(5), 2566 (2023)